THE ASTROPHYSICAL JOURNAL, 564:369–378, 2002 January 1


# GAMMA-RAY EMISSION FROM AN OUTER GAP ACCELERATOR: CONSTRAINTS ON MAGNETOSPHERIC CURRENT, MAGNETIC INCLINATION, AND DISTANCE FOR PSR B1055−52

KOUICHI HIROTANI
NASA Goddard Space Flight Center, Laboratory for High Energy Astrophysics, Code 661, Greenbelt, MD 20771; hirotani@milkyway.gsfc.nasa.gov
AND
SHINPEI SHIBATA
Department of Physics, Yamagata University, Yamagata 990-8560, Japan; shibata@sci.kj.yamagata-u.ac.jp
*Received 2001 May 31; accepted 2001 September 5*

## ABSTRACT

We investigate a stationary pair production cascade in the outer magnetosphere of a spinning neutron star. The charge depletion due to global flows of charged particles causes a large electric field along the magnetic field lines. Migratory electrons and/or positrons are accelerated by this field to radiate curvature $\gamma$-rays, some of which collide with the X-rays to materialize as pairs in the gap. The replenished charges partially screen the electric field, which is self-consistently solved, together with the distribution functions of particles and $\gamma$-rays. By solving the Vlasov equations describing this pair production cascade, we demonstrate the existence of a stationary gap in the outer magnetosphere of PSR B1055−52 for a wide range of current densities flowing in the accelerator: from sub– to super–Goldreich-Julian values. However, we find that the expected GeV spectrum becomes very soft if the current density exceeds the Goldreich-Julian value. We also demonstrate that the GeV spectrum softens with decreasing magnetic inclination and with increasing distance to this pulsar. We thus conclude that a sub–Goldreich-Julian current, a large magnetic inclination, and a small distance (500 pc, say) are plausible to account for EGRET observations. Furthermore, it is found that the TeV flux due to inverse Compton scatterings of infrared photons whose spectrum is inferred from the Rayleigh-Jeans side of the soft blackbody spectrum is much less than the observational upper limit.

*Subject headings:* gamma rays: observations — gamma rays: theory — pulsars: individual (PSR B1055−52) — stars: magnetic fields — X-rays: stars

## 1. INTRODUCTION

The EGRET experiment on the *Compton Gamma Ray Observatory* has detected pulsed signals from seven rotation-powered pulsars (for the Crab pulsar, see Nolan et al. 1993; Fierro et al. 1998; for the Vela pulsar, see Kanbach et al. 1994; Fierro et al. 1998; for Geminga, see Mayer-Hasselwander et al. 1994; Fierro et al. 1998; for PSR B1706−44, see Thompson et al. 1996; for PSR B1046−58, see Kaspi at al. 2000; for PSR B1055−52, see Thompson et al. 1999; for PSR B1951+32, see Ramanamurthy et al. 1995). The modulation of the $\gamma$-ray light curves at GeV energies testifies to the production of $\gamma$-ray radiation in the pulsar magnetospheres at either the polar cap (Harding, Tademaru, & Esposito 1978; Daugherty & Harding 1982, 1996; Michel 1991; Sturner, Dermer, & Michel 1995; Shibata, Miyazaki, & Takahara 1998; Harding & Muslimov 1998; Zhang & Harding 2000) or the vacuum gaps in the outer magnetosphere (see, e.g., Cheng, Ho, & Ruderman 1986a, 1986b, hereafter CHRa and CHRb, respectively). Both of these pictures have had some success in reproducing global properties of the observed emission. However, there is an important difference between these two models: a polar gap accelerator releases very little angular momenta, while an outer gap one could radiate them efficiently. More specifically, the total angular momentum loss rate must equal the energy loss rate divided by the angular velocity of the star, implying an average location of energy loss on the light cylinder (Cohen & Treves 1972; Holloway 1977; Shibata 1995), from which the distance from the rotation axis is given by

$$\varpi_{\rm LC} = \frac{c}{\Omega}, \tag{1}$$

where $\Omega$ denotes the angular frequency of the neutron star and $c$ the speed of light.

On these grounds, the purpose here is to explore further a model of an outer gap, which is located near the light cylinder. If the outer magnetosphere is filled with a plasma so that the space charge density is equal to the Goldreich-Julian density, $\rho_{\rm GJ} \equiv -\Omega B_z/(2\pi c)$, then the field-aligned electric field vanishes, where $B_z$ is the component of the magnetic field along the rotational axis. However, the depletion of charge in the Goldreich and Julian model in a region where it could not be resupplied may cause a vacuum region to develop. Holloway (1973) pointed out the possibility that a region that lacks plasma is formed around the surface on which $\rho_{\rm GJ}$ changes its sign. Subsequently, CHRa and CHRb developed a version of an outer magnetospheric $\gamma$-ray emission zone in which acceleration in the Holloway gaps above the null surface, where $B_z$ vanishes, brought particles to large Lorentz factors ($\sim 10^{7.5}$).

After CHRa and CHRb, many outer gap models have been proposed (Chiang & Romani 1992, 1994; Romani & Yadigaroglu 1995; Romani 1996; Zhang & Cheng 1997; Cheng, Ruderman, & Zhang 2000). Their basic idea is as follows: A deviation of the charge density from $\rho_{\rm GJ}$ results in an electric field along the magnetic field $\boldsymbol{B}$. If this electric field becomes strong enough to accelerate $e^{\pm}$ pairs to

ultrarelativistic energies, they could radiate $\gamma$-rays tangential to the curved $\boldsymbol{B}$ field lines there. The curvature $\gamma$-rays may be converted into $e^{\pm}$ pairs via two photon collisions. In order to keep a steady current flow and the charge density $\rho_{\rm GJ}$ in the regions outside the gap, the gap will grow until it is large enough and the electric field is strong enough to maintain a sufficient supply of charges to the rest of the open field line region. If the gap ends in a region where $\rho_{\rm GJ} \neq 0$ and $\boldsymbol{E} \cdot \boldsymbol{B} \neq 0$, charges from the surrounding region may flow in through the end (or the boundary). If both boundaries are located on the null surface, pairs produced in the gap will replace the charge deficiency inside the gap, and finally the gap will be filled up. However, if a vacuum gap extends to the light cylinder, the charged particles created in the gap should escape from the magnetosphere, so the gap would not be quenched. Hence, stable outer gaps (if they exist) are those from the null surface to the light cylinder along the last open field lines. In an outer gap, the inner boundary lies near the intersection of the null surface where $\rho_{\rm GJ}$ vanishes and the boundary of the closed field lines of the star on which the magnetospheric current does not exits.

Recently, solving the Vlasov equations that describe a stationary pair production cascade, Hirotani & Shibata (2001a, 2001b, hereafter Papers VII and VIII, respectively) elucidated important characteristics of the particle acceleration zones in the outer magnetosphere. They demonstrated that a stationary gap does not extend between the null surface and the light cylinder. Rather, their width ($W$) along the field lines is adjusted so that a single particle emits copious $\gamma$-rays, one of which materializes as a pair in the gap on average. The resultant $W$ becomes about 5% of $\varpi_{\rm LC}$ in the case of the Crab pulsar. The produced pairs in the gap do not completely cancel the acceleration field because the particles do not accumulate at the gap boundaries. Outside of the gap, the particles flow away from the gap along the magnetic field lines as a part of the global current flow pattern. In other words, the remaining small-amplitude electric field along the magnetic field lines outside of the gap prevents the gap from quenching. Moreover, they demonstrated that the gap position is not fixed, as was considered in previous outer gap models. Their position shifts as the magnetospheric current flowing in the gap changes. That is, if there is no particle injection across either of the boundaries, the gap is located around the null surface, as demonstrated in their earlier papers (Hirotani & Shibata 1999a, 1999b, 1999c, hereafter Papers I, II, and III, respectively; Hirotani 2000a, 2000b, 2001, hereafter Papers IV, VI, and V, respectively; see also Beskin, Istomin, & Par'ev 1992 and Hirotani & Okamoto 1998 for a pair production avalanche in a black hole magnetosphere). However, the gap position shifts toward the light cylinder (or the star surface) if the injected particle flux across the inner (or the outer) boundary approaches the Goldreich-Julian value. In other words, the accelerator can be located at any place in the magnetosphere; its position is primarily constrained by the magnetospheric current.

In Papers VII and VIII, they examined the outer gaps formed in the magnetospheres of young or millisecond pulsars, assuming a sub–Goldreich-Julian particle injection across the boundaries. In this paper, we apply the same method to the middle-aged pulsar B1055$-$52 and demonstrate that a stationary gap is maintained even if the injected particle flux exceeds the Goldreich-Julian value and that the possibility of such a large particle flux injection is ruled out if we compare the predicted $\gamma$-ray spectrum with observations.

In the next section, we formulate the basic equations describing the stationary pair production cascade in the outer magnetosphere. In § 3, we apply the method to the middle-aged pulsar, B1055$-$52 and reveal that large magnetic inclination and a sub–Goldreich-Julian current are plausible for the outer magnetospheric emission from this pulsar. In the final section, we compare the results with previous works.

## 2. BASIC EQUATIONS

We first consider the continuity equations of particles in § 2.1 and the Boltzmann equations of $\gamma$-rays in § 2.2. Combining these equations with the Poisson equation, we present the Vlasov equations describing the one-dimensional electrodynamic structure of an accelerator along the field lines in § 2.3. We finally give appropriate boundary conditions in § 2.4.

### 2.1. *Particle Continuity Equations*

In the same manner as in Papers I–VIII, we simply assume that the electrostatic and curvature radiation reaction forces cancel each other in the Boltzmann equations of particles. Under this monoenergetic approximation, the Boltzmann equations reduce to continuity equations. Assuming that the toroidal bending is negligible for the magnetic field, we obtain the following stationary ($\partial_t + \Omega\partial_\phi = 0$) continuity equations (Paper VII):

$$\pm B \frac{d}{ds}\left(\frac{N_\pm}{B}\right) = \frac{1}{c}\int_0^\infty d\epsilon_\gamma (\eta_{p+} G_+ + \eta_{p-} G_-) , \qquad (2)$$

where $N_+$ and $N_-$ represent the spatial densities of positrons and electrons, respectively, $G_+$ and $G_-$ the distribution functions of outwardly and inwardly propagating $\gamma$-rays, respectively, and $B$ the strength of the magnetic field. The pair production redistribution functions $\eta_{p\pm}$ can be defined as

$$\eta_{p\pm}(\epsilon_\gamma) = (1-\mu_c)c \int_{\epsilon_{\rm th}}^\infty d\epsilon_{\rm X} \frac{dN_{\rm X}}{d\epsilon_{\rm X}} \sigma_p(\epsilon_\gamma, \epsilon_{\rm X}, \mu_c) , \qquad (3)$$

where $\sigma_p$ is the pair production cross section and $\cos^{-1}\mu_c$ refers to the collision angle between the $\gamma$-rays and the X-rays with energy $m_e c^2 \epsilon_{\rm X}$. The X-ray number density between dimensionless energies $\epsilon_{\rm X}$ and $\epsilon_{\rm X} + d\epsilon_{\rm X}$ is integrated over $\epsilon_{\rm X}$ above the threshold energy $\epsilon_{\rm th} \equiv 2(1-\mu_c)^{-1}\epsilon_\gamma^{-1}$ to infinity.

In Paper VII, we adopted $\mu_c = \cos(W/\varpi_{\rm LC})$ for the Crab pulsar magnetosphere, in which a power-law X-ray component dominates the surface ones. However, in the present paper, we apply the theory to the middle-aged pulsar B1055$-$52, for which soft X-ray emission is dominated by surface components. We thus evaluate $\mu_c$ by the collision angle between the *surface* X-rays and the curvature $\gamma$-rays. The collision approaches head-on (or tail-on) for inwardly (or outwardly) propagating $\gamma$-rays as the gap shifts toward the star.

### 2.2. *Boltzmann Equations for Gamma Rays*

For simplicity, we assume that the outwardly (or inwardly) propagating $\gamma$-rays dilate (or constrict) at the same rate as the magnetic field; this assumption gives a

good estimate when $W \ll \varpi_{\rm LC}$ holds. Under this assumption, we obtain (Paper VII)

$$\pm B \frac{\partial}{\partial s}\left(\frac{G_\pm}{B}\right) = -\frac{\eta_{p\pm}}{c} G_\pm + \frac{\eta_c}{c} N_\pm , \quad (4)$$

where the redistribution function $\eta_c$ for the curvature radiation is explicitly defined in equation (12) in Paper VII (see also Rybicki & Lightman 1979).

### 2.3. *One-Dimensional Analysis*

As described at the end of § 3 in Paper VII, it is convenient to introduce the Debey scale length $c/\omega_p$, where

$$\omega_p = \sqrt{\frac{4\pi e^2}{m_e}\frac{\Omega B_{\rm cnt}}{2\pi c e}} , \quad (5)$$

and $B_{\rm cnt}$ is the magnetic field strength at the gap center. The dimensionless coordinate variable then becomes

$$\xi \equiv (\omega_p/c)s . \quad (6)$$

By using such dimensionless quantities and by assuming that the transfield thickness of the gap is greater than $W$, we can rewrite the Poisson equation into the following one-dimensional form (Paper VII):

$$E_\parallel = -\frac{d\psi}{d\xi} , \quad (7)$$

$$\frac{dE_\parallel}{d\xi} = \frac{B(\xi)}{B_{\rm cnt}}[n_+(\xi) - n_-(\xi)] + \frac{B_z(\xi)}{B_{\rm cnt}} , \quad (8)$$

where $\psi(\xi) \equiv e\Psi(s)/(m_e c^2)$; the particle densities are normalized by the Goldreich-Julian value as

$$n_\pm(\xi) \equiv \frac{2\pi c e}{\Omega}\frac{N_\pm}{B} . \quad (9)$$

We evaluate $B_z/B$ at each point along the last open field line by using the Newtonian dipole field.

Let us introduce the following dimensionless $\gamma$-ray densities in the dimensionless energy interval between $\beta_{i-1}$ and $\beta_i$:

$$g^i_\pm(\xi) \equiv \frac{2\pi c e}{\Omega B_{\rm cnt}} \int_{\beta_{i-1}}^{\beta_i} d\epsilon_\gamma G_\pm(s, \epsilon_\gamma) . \quad (10)$$

In this paper, we set $\beta_0 = 10^2$, which corresponds to the lowest $\gamma$-ray energy, 51.1 MeV. We divide the $\gamma$-ray spectra into 11 energy bins and put $\beta_1 = 10^{2.5}$, $\beta_2 = 10^3$, $\beta_3 = 10^{3.25}$, $\beta_4 = 10^{3.5}$, $\beta_5 = 10^{3.75}$, $\beta_6 = 10^4$, $\beta_7 = 10^{4.25}$, $\beta_8 = 10^{4.5}$, $\beta_9 = 10^{4.75}$, $\beta_{10} = 10^5$, and $\beta_{11} = 10^{5.25}$. We can now rewrite the continuity equation (eq. [2]) of particles into

$$\frac{dn_\pm}{d\xi} = \pm \frac{B_{\rm cnt}}{B} \sum_{i=1}^{9} [\eta^i_{p+} g^i_+(\xi) + \eta^i_{p-} g^i_-(\xi)] , \quad (11)$$

where the magnetic field strength $B$ is evaluated at each $\xi$. The dimensionless redistribution functions $\eta^i_{p\pm}$ are evaluated at the central energy in each bin as

$$\eta^i_{p\pm} \equiv \frac{1}{\omega_p}\eta_{p\pm}\left(\frac{\beta_{i-1} + \beta_i}{2}\right) . \quad (12)$$

A combination of equation (11) gives the current conservation law,

$$j_{\rm tot} \equiv n_+(\xi) + n_-(\xi) = \text{constant for } \xi . \quad (13)$$

If $j_{\rm tot} = 1$ holds, the current density per unit magnetic flux tube equals the Goldreich-Julian value $\Omega/(2\pi)$.

The Boltzmann equation (eq. [4]) for the $\gamma$-rays is integrated over $\epsilon_\gamma$ between dimensionless energies $\beta_{i-1}$ and $\beta_i$ to become

$$\frac{d}{d\xi} g^i_\pm = \frac{d}{d\xi}(\ln B) g^i_\pm \mp \eta^i_{p\pm} g^i_\pm \pm \frac{\eta^i_c B(\xi)}{B_{\rm cnt}} n_\pm , \quad (14)$$

where $i = 1, 2, \ldots, m$ ($m = 9$) and

$$\eta^i_c \equiv \frac{\sqrt{3}e^2\Gamma}{\omega_p h R_C}\int_{\beta_{i-1}/\epsilon_c}^{\beta_i/\epsilon_c} du \int_u^\infty K_{(5/3)}(t)dt \quad (15)$$

is dimensionless and $K_{5/3}$, $R_C$, and $\Gamma$ refer to the modified Bessel function of 5/3 order, curvature radius of the magnetic field lines, and the particle Lorentz factor, respectively.

To ensure that the Lorentz factors do not exceed the maximum attainable limit $\psi(\xi_2)$, we compute $\Gamma$ with (Paper VII)

$$\frac{1}{\Gamma} = \sqrt{\frac{1}{\Gamma^2_{\rm sat}} + \frac{1}{\psi^2(\xi_2)}} , \quad (16)$$

where

$$\Gamma_{\rm sat} \equiv \left(\frac{3R_C^2}{2e}\left|\frac{d\Psi}{ds}\right| + 1\right)^{1/4} ; \quad (17)$$

represents the terminal Lorentz factor that is realized if the electric force $e|d\Psi/dx|$ balances with the radiation reaction force.

### 2.4. *Boundary Conditions*

We now consider the boundary conditions to solve the Vlasov equations (eqs. [7], [8], [11], and [14]). At the *inner* (starward) boundary ($\xi = \xi_1$), we impose (Paper VII)

$$E_\parallel(\xi_1) = 0 , \quad (18)$$

$$\psi(\xi_1) = 0 , \quad (19)$$

$$g^i_+(\xi_1) = 0, \quad (i = 1, 2, \ldots, 9) , \quad (20)$$

$$n_+(\xi_1) = j_1 , \quad (21)$$

where the dimensionless positronic current at $\xi = \xi_1$ is denoted as $j_1$. Note that equations (13) and (21) yield

$$n_-(\xi_1) = j_{\rm tot} - j_1 . \quad (22)$$

At the *outer* boundary ($\xi = \xi_2$), we impose

$$E_\parallel(\xi_2) = 0 , \quad (23)$$

$$g^i_-(\xi_2) = 0, \quad (i = 1, 2, \ldots, 9) , \quad (24)$$

$$n_-(\xi_2) = j_2 . \quad (25)$$

The current density created in the gap per unit flux tube can be expressed as

$$j_{\rm gap} = j_{\rm tot} - j_1 - j_2 . \quad (26)$$

We adopt $j_{\rm gap}, j_1$, and $j_2$ as the free parameters.

We have totally $2m + 6$ boundary conditions (eqs. [18]–[25]) for $2m + 4$ unknown functions $\Psi$, $E_\parallel$, $n_\pm$, and $g^i_\pm$ ($i = 1, 2, \ldots, m$), where $m = 11$. Thus, two extra boundary conditions must be compensated by making the positions of

the boundaries $\xi_1$ and $\xi_2$ be free. The two free boundaries appear because $E_\parallel = 0$ is imposed at *both* the boundaries and because $j_{\rm gap}$ is externally imposed (see § 4.1 for details). In other words, the gap boundaries ($\xi_1$ and $\xi_2$) shift if $j_1$ and/or $j_2$ varies.

It is worth mentioning that the gap width $W$ is related to the X-ray field density as follows (for details, see Papers V, VII, and VIII):

$$W = \frac{\lambda_p}{N_\gamma} \frac{j_{\rm gap}}{j_{\rm tot}}, \tag{27}$$

where $\lambda_p$ refers to the pair production optical depth and $N_\gamma$ the expectation value of the $\gamma$-ray photons emitted by a single particle while it runs the gap. Equation (27) is automatically satisfied by the stationary Vlasov equations. From equation (27), we can expect an extended gap for middle-aged pulsars because their less dense X-ray field leads to a large $\lambda_p$ and hence a large $W$ compared to young pulsars like Crab. We examine such features more accurately in the next section by analyzing the Vlasov equations numerically.

## 3. APPLICATION TO PSR B1055−52

### 3.1. *X-Ray and Infrared Field*

Combining *ROSAT* and *ASCA* data, Greiveldinger et al. (1996) reported that the X-ray spectrum consists of two components: a soft blackbody with $kT_s = 68$ eV and $A_s = 0.78 A_*(d/0.5)^2$ and a hard blackbody with $kT_h = 320$ eV and $A_h = (2.5 \times 10^{-5}) A_*(d/0.5)^2$, where $d$ refers to the distance in kiloparsecs. Here, $A_s$ and $A_h$ indicate the observed emission area of soft and hard blackbody components, respectively; $A_*$ expresses the area of the whole neutron star surface.

Mignani, Caraveo, & Bignami (1997) claimed that the blue/UV flux is consistent with an extrapolation of the soft, thermal part of the *ROSAT* X-ray spectrum. We thus compute the infrared flux from the Rayleigh-Jeans side of the soft X-ray spectrum with $kT_s = 68$ eV and $A_s = 0.78 A_*(d/0.5)^2$. This IR photon field is, in fact, so weak that the inverse Compton drag acting on a particle is negligibly small compared to the curvature drag. Therefore, the Vlasov equations can be solved without the IR field (i.e., the pair production rate can be computed only from the GeV-keV collisions).

### 3.2. *Dependence on Injected Currents*

Let us now substitute the X-ray field into equation (3) and solve the Vlasov equations by the method described in § 2. Once $E_\parallel(\xi)$, $n_\pm(\xi)$, and $g^i_\pm(\xi)$ are solved, we can compute the GeV and TeV spectra by the method described in § 4 in Paper VII.

#### 3.2.1. *Equal Current Injection*

We first consider the case in which $j_1 = j_2$. In Figure 1, we present the acceleration field,

$$-\frac{d\Psi}{ds} = \frac{\omega_p}{c} \frac{m_e c^2}{e} E_\parallel, \tag{28}$$

for four cases: $j_1 = j_2 = 0$, 0.005, 0.05, and 2.0, which are indicated by the solid, dashed, dot-dashed, and dotted curves, respectively. In the third case, for instance, the positronic and electronic currents flow equally into the gap across the inner and outer boundaries at the rate $0.05\Omega/2\pi$ per unit magnetic flux tube (i.e., 5% of the typical Goldreich-Julian value). For all four cases, we set $\alpha_i = 60°$. Since the space charge is overfilled (or equivalently, $-d\Psi/ds$ distribution forms a brim as described in Hirotani & Okamoto 1998; see § 4.2 for details) if $j_{\rm gap}$ exceeds typically several percent, we adopt $j_{\rm gap} = 0.01$ as the representative value. The abscissa designates the distance along the last open field line and covers the range from the neutron star surface ($s = 0$) to the position where the distance equals $s = 0.35\varpi_{\rm LC} = 3.29 \times 10^6$ m.

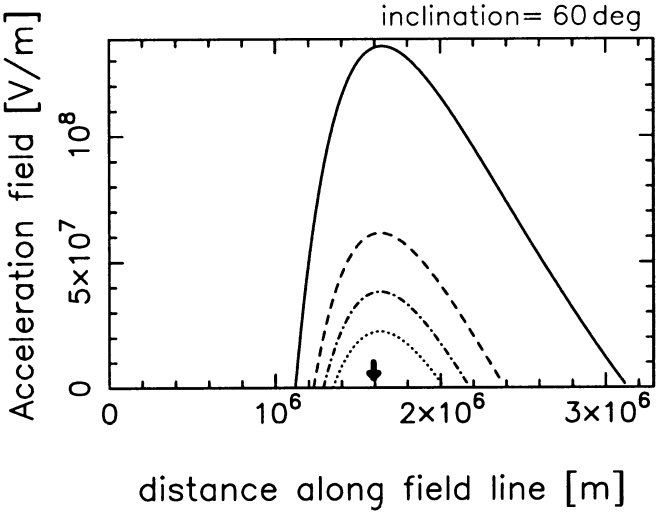


FIG. 1.—Distribution of the acceleration field, $-d\Psi/ds$, for PSR B1055−52 for $\alpha_i = 60°$. The solid, dashed, dot-dashed, and dotted curves correspond to the cases of $(j_{\rm gap}, j_1, j_2) = (0.01, 0, 0)$, $(0.01, 0.005, 0.005)$, $(0.01, 0.05, 0.05)$, and $(0.01, 2, 2)$, respectively. The arrow indicates the position of the null surface where $B_z$ vanishes.

It follows from Figure 1 that the gap is located around the null surface (where $B_z$ vanishes), which is indicated by the arrow. For $\alpha_i = 60°$, $\Omega = 31.9$ rad s$^{-1}$, the null surface is located at $s = 1.59 \times 10^6$ m from the star surface along the last open field line. The conclusion that the gap is located around the null surface for $j_1 = j_2$ is consistent with what was obtained analytically in § 2.4 in Paper VII. We can also understand from Figure 1 that $W$, and hence $-d\Psi/ds$, decreases with increasing $j_1 = j_2$. This is because not only the produced particles in the gap (i.e., $j_{\rm gap}$) but also the injected ones (i.e., $j_1 + j_2$) contribute to the $\gamma$-ray emission. Because of the efficient $\gamma$-ray emission due to the injected particles, a stationary pair production cascade is maintained with a small pair production optical depth $W/\lambda_p$ and hence a small $W$. It is noteworthy that $W$ does not linearly decrease with $j_{\rm gap}/j_{\rm tot}$ by virtue of the "negative feedback effect" due to the $N_\gamma^{-1}$ factor; that is, the decrease in $N_\gamma$ due to the reduced $W$ partially cancels the original decrease in $W$. It may be noteworthy that $N_\gamma \propto W\Gamma \propto W^{3/2}$ holds (for details, see eqs. [8], [11], and [31] in Paper V, along with Fig. 6 in Hirotani & Okamoto 1998).

We present the $\gamma$-ray spectrum in Figure 2; the curves correspond to the same cases as those in Figure 1. In each case, outwardly propagating $\gamma$-ray flux is depicted because it is greater than the inwardly propagating one. The observed fluxes are indicated by open circles and squares. It follows that the spectrum becomes soft as the injected current densities, $j_1 = j_2$, increase. This can be easily understood because $-d\Psi/ds$ decreases with increasing $j_1 = j_2$ (Fig. 1). Even though solutions exist for super–Goldreich-

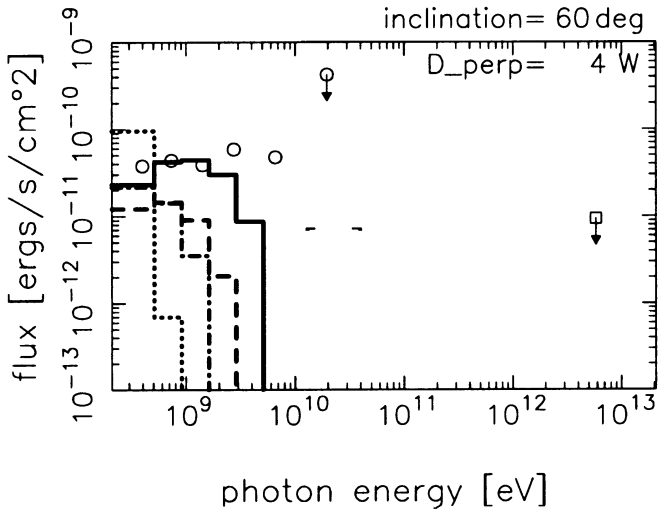


FIG. 2.—Expected pulsed γ-ray spectra from PSR B1055−52 for $\alpha_i = 60°$ and $j_{gap} = 0.01$. The four curves correspond to the same cases as presented in Fig. 1. In each case, the larger flux for either the inwardly or the outwardly propagating γ-rays is depicted.

Julian currents (e.g., the dotted line in Fig. 2), the predicted spectra become too soft to match the observations. On these grounds, we can conclude that *a sub–Goldreich-Julian current density is preferable for us to account for the observed spectrum.*

### 3.2.2. *Current Injection across the Outer Boundary*

We next consider the case in which the gap is shifted toward the star surface by virtue of the particle injection across the outer boundary. In Figure 3, we present $-d\Psi/ds$ for vanishing $j_1$; the solid, dashed, and dotted curves represent the cases of $(j_1, j_2) = (0, 0)$, $(0, 0.25)$, and $(0, 0.391)$, respectively. For all three cases, we set $\alpha_i = 60°$ and $j_{gap} = 0.01$. The abscissa covers the range from $s = 0$ to $s = 0.35\varpi_{LC}$. There is no solution above $j_2 > 0.391$ because the space charge is overfilled at the inner boundary above this critical value.

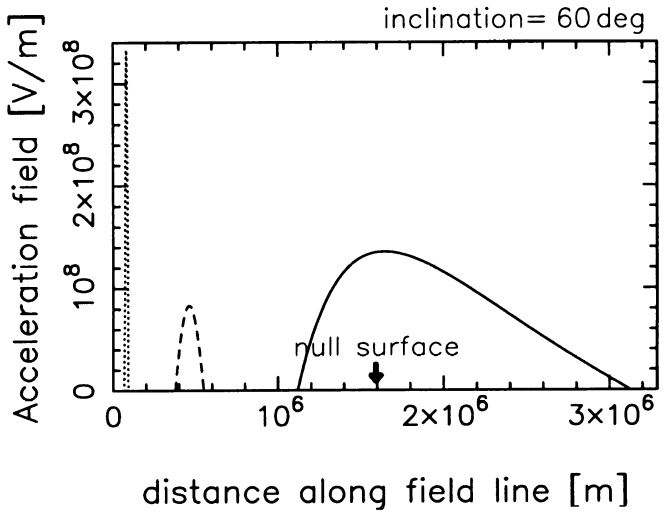


FIG. 3.—Distribution of $-d\Psi/ds$ for PSR B1055−52 for $\alpha_i = 60°$. The solid, dashed, and dotted curves correspond to the cases of $(j_{gap}, j_1, j_2) = (0.01, 0, 0)$, $(0.01, 0, 0.25)$, and $(0.01, 0, 0.391)$, respectively.

It follows from the figure that the gap position shifts inward as $j_2$ increases. For example, the gap center position shifts from $0.225\varpi_{LC}$ for $j_2 = 0$ (*solid curve*) to $0.049\varpi_{LC}$ and $0.0084\varpi_{LC}$ for $j_2 = 0.25$ (*dashed curve*) and $j_2 = 0.391$ (*dotted curve*), respectively, from the star surface along the last open field line. In addition, $W$ decreases significantly as the gap shifts inward. This is because both the factors $j_{gap}/j_{tot}$ and $\lambda_p$ decreases in equation (27). For details, see § 6.1 in Paper VII.

Let us now consider the Lorentz factor. As the maximum value in the gap, we obtain $3.0 \times 10^7$ for $j_2 = 0$ (*solid curve*), whereas $8.7 \times 10^6$ for $j_2 = 0.391$ (*dotted curve*). That is, in the latter case, $\Gamma$ reduces significantly even though the maximum of $-d\Psi/ds$ is greater than the former. This is because the particles' motion becomes unsaturated because of the reduced $W$. Therefore, the monoenergetic approximation is no longer valid for the dotted curve in Figure 3.

The emitted spectra are presented in Figure 4. Because the Lorentz factor decreases as $j_2$ increases, the spectrum becomes soft as the gap shifts inward. For the dotted curve, the spectrum would be further softened from Figure 4 if we considered the unsaturated effect of particle motion. We can therefore conclude that the gap should not be located well inside of the null surface for $\alpha_i \approx 60°$ so that the predicted GeV spectrum may not be significantly inconsistent with observations.

### 3.2.3. *Current Injection across the Inner Boundary*

Let us consider the case in which the gap shifts toward the light cylinder as a result of the particle injection across the inner boundary. In Figure 5, we present $-d\Psi/ds$ for vanishing $j_2$; the solid, dashed, dot-dashed, and dotted curves represent the cases of $(j_1, j_2) = (0, 0)$, $(0.25, 0)$, $(0.5, 0)$, and $(0.585, 0)$, respectively. For all four cases, we set $\alpha_i = 60°$ and $j_{gap} = 0.01$. The abscissa covers the range from $s = 0$ to $s = 1.3\varpi_{LC}$. There is no solution above $j_1 > 0.585$ because the space charge is overfilled at the outer boundary above this critical value.

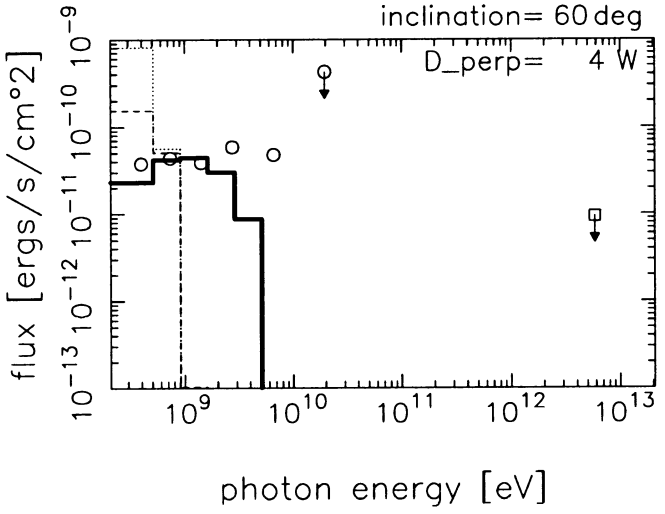


FIG. 4.—Expected pulsed γ-ray spectra from PSR B1055−52 for $\alpha_i = 60°$, $j_{gap} = 0.01$, and $j_1 = 0$. The four curves correspond to the same cases as presented in Fig. 3. In each case, the larger flux for either the inwardly or the outwardly propagating γ-rays is depicted. If the curve is thick (or thin), it means that the outwardly (or inwardly) propagating γ-ray flux is greater than the other.

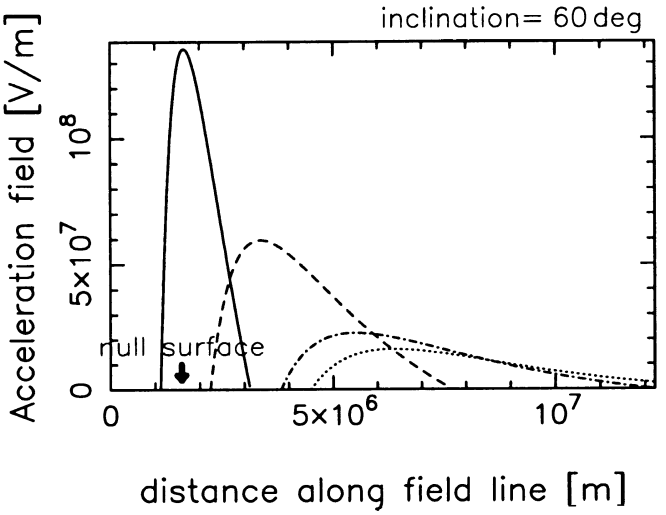


FIG. 5.—Distribution of $-d\Psi/ds$ for PSR B1055−52 for $\alpha_i = 60°$. The solid, dashed, dot-dashed, and dotted curves correspond to the cases of $(j_{\rm gap}, j_1, j_2) = (0.01, 0, 0)$, $(0.01, 0.25, 0)$, $(0.01, 0.5, 0)$, and $(0.01, 0.585, 0)$, respectively.

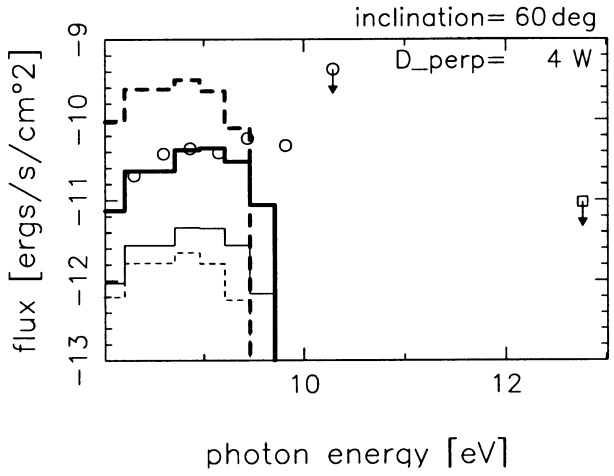


FIG. 7.—Expected pulsed $\gamma$-ray spectra from PSR B1055−52 for $\alpha_i = 60°$, $j_{\rm gap} = 0.01$, and $j_2 = 0$. The solid and dashed lines correspond to $j_1 = 0$ and $j_1 = 0.25$, respectively, while the thick and thin lines correspond to the outwardly and inwardly propagating flux at $\xi = \xi_2$ and $\xi_1$, respectively.

It follows from the figure that the gap shifts outward as $j_1$ increases. For example, the gap center is located at $s = s_{\rm cnt} \equiv (s_1 + s_2)/2 = 0.225\varpi_{\rm LC}$ for $j_1 = 0$ (*solid curve*), while it shifts to the position $s = 0.526\varpi_{\rm LC}$ and $s = 0.854\varpi_{\rm LC}$ for $j_1 = 0.25$ (*dashed curve*) and $j_1 = 0.5$ (*dot-dashed curve*), respectively. In addition, $W$ increases as the gap shifts outward. This is because the diluted X-ray field at the outer part of the gap increases $\lambda_p$ (see eq. [27]). The increase of $W$ with increasing $j_1$, however, does not mean that $-d\Psi/ds$ increases with $j_1$. This is because the small $|\rho_{\rm GJ}| \propto |B_z| \sim r^{-3}$ at larger distance from the star results in a small $|d(-d\Psi/ds)/ds|$ in the Poisson equation.

The emitted spectra are presented in Figure 6. The curvature spectrum becomes the hardest for $(j_1, j_2) = (0, 0)$ of the four cases because $-d\Psi/ds$ becomes large by virtue of the strong magnetic field at relatively small distance from the star. It follows from the solid and dashed curves in Figures 4 and 6 that the spectrum does not soften very rapidly when $j_1$ increases (Fig. 6) compared to the case in which $j_2$ increases (Fig. 4). This is because $W$ increases with increasing $j_1$ (Fig. 5), while it significantly decreases with increasing $j_2$ (Fig. 3).

In passing, it is worth examining the relative magnitudes of the inward and outward fluxes. We consider the two cases $j_1 = 0$ (*solid curve*) and 0.25 (*dashed curve*) for $\alpha_i = 60°$, $j_{\rm gap} = 0.01$, and $j_2 = 0$ in Figure 7. The thick (or thin) lines denote the $\nu F_\nu$ fluxes of outwardly (or inwardly) propagating $\gamma$-rays at the outer (or inner) boundary. Because of the $r^{-2}$ factor in the soft photon flux, the pair production is active at the inner part of the gap. Thus, the positron (or electron) density rapidly increases (or decreases) with increasing $\xi$ at the inner part and nearly saturates at $j_{\rm tot}$ (or $j_2$) in the outer part. See Figure 8 for the $n_+$ (thick) and $n_-$ (thin) distribution for $\alpha_i = 60°$, $j_{\rm gap} = 0.01$, and $j_1 = j_2 = 0$.

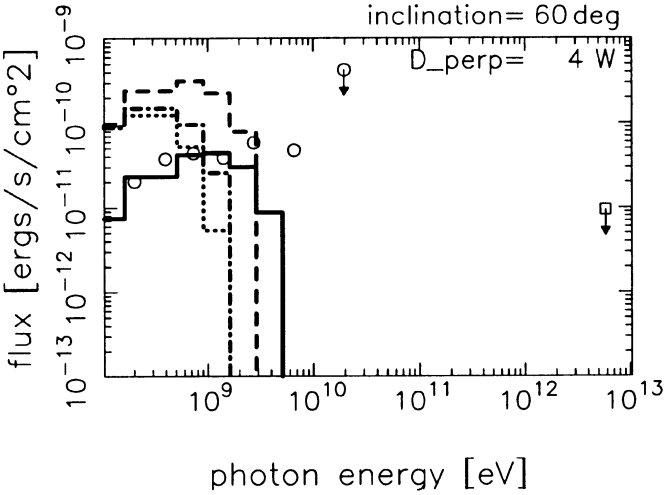


FIG. 6.—Expected pulsed $\gamma$-ray spectra from PSR B1055−52 for $\alpha_i = 60°$, $j_{\rm gap} = 0.01$, and $j_2 = 0$. The solid, dashed, dot-dashed, and dotted curves correspond to the cases of $j_1 = 0$, 0.25, 0.5, and 0.5847, respectively. Since the outward $\gamma$-ray flux dominates the inward one in each case, the former is depicted.

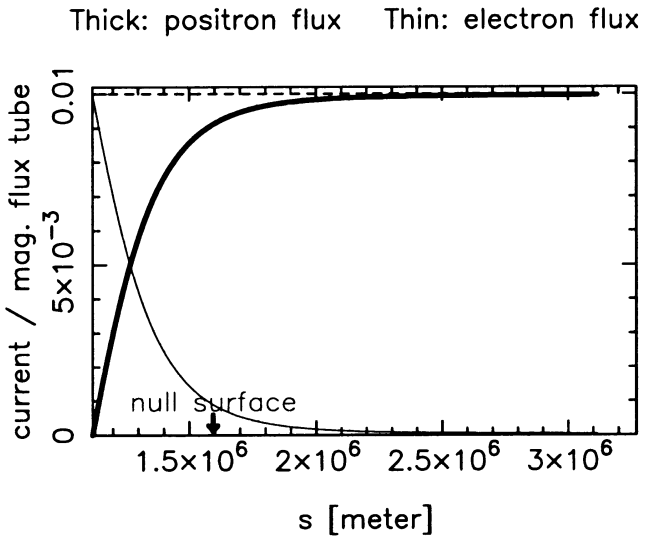


FIG. 8.—Positronic (*thick curve*) and electronic (*thin curve*) density distribution in the outer gap of PSR B1055−52 for $\alpha_i = 60°$, $j_{\rm gap} = 0.01$, and $j_1 = j_2 = 0$.

Because of this asymmetric distribution of $n_+$ and $n_-$ along $\xi$, outwardly propagating $\gamma$-ray flux dominates the inwardly propagating one. It is noteworthy that the *extended* gap for this middle-aged pulsar results in this large asymmetry. For a small gap (i.e., $W \ll \varpi_{LC}$) obtained for young pulsars (Papers VII and VIII) and supermassive black holes (Hirotani & Okamoto 1998), the flux ratio between the outwardly and inwardly propagating $\gamma$-rays are slightly less than unity because $n_+$ and $n_-$ distribute almost symmetrically with respect to the gap center.

It also follows from Figure 7 that the outward $\gamma$-ray flux dominates the inward one when $j_1$ increases. This is because the injected positron at the inner boundary also contributes to the $\gamma$-ray emission.

Let us summarize the main points that have been made in §§ 3.2.1–3.2.3. The curvature spectrum becomes the hardest when $j_1 = j_2 = 0$. In this case, the gap is located close to the null surface, where $B_z$ vanishes.

### 3.3. *Dependence on Inclination*

It has been revealed that the $\gamma$-ray spectrum becomes hardest when the injected current is small (say, when $j_1 \sim j_2 \sim 0$) and that the EGRET spectrum cannot be explained for $\alpha_i = 60°$ (as the solid lines in Figs. 2, 4, and 6 indicate). Since the $\gamma$-ray energies are predicted to increase with increasing $\alpha_i$ in Paper V, we examine in this section whether the EGRET pulsed flux around 6 GeV can be explained if we consider a larger $\alpha_i$. In Figures 9 and 10, we present the acceleration fields and the expected spectra for $\alpha_i = 80°$, 75°, 60°, and 45° as the dot-dashed, dashed, solid, and dotted lines, respectively. The current densities are chosen as $j_{gap} = 0.01$ and $j_1 = j_2 = 0$. In each case, the outward $\gamma$-ray flux is depicted because it dominates the inward ones.

It follows from Figure 10 that a large inclination angle (75° or greater) is preferable to explain the $\gamma$-ray spectrum around 6 GeV. The reasons are fourfold (see also § 6.2 in Paper VII):

1. The distance of the null surface from the star decreases with increasing $\alpha_i$.

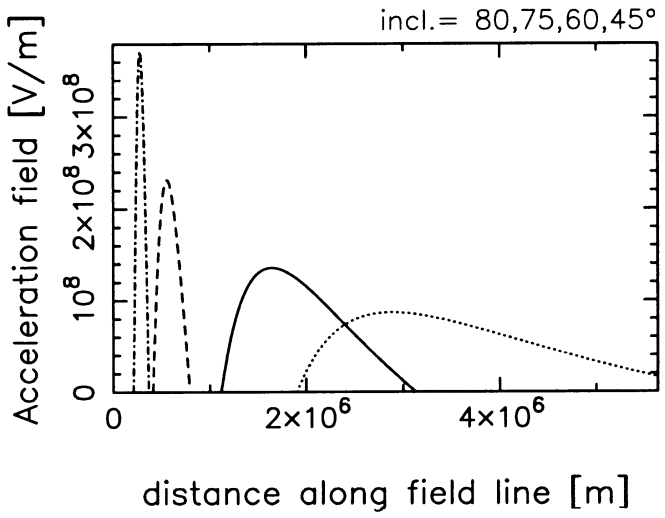


FIG. 9.—Distribution of $-d\Psi/ds$ for PSR B1055−52 for $\alpha_i = 80°$(*dot-dashed curve*), 75° (*dashed curve*), 60° (*solid curve*), and 45° (*dotted curve*). The current densities are fixed as $j_{gap} = 0.01$ and $j_1 = j_2 = 0$; therefore, the peak of each curve corresponds to the null surface for each inclination.

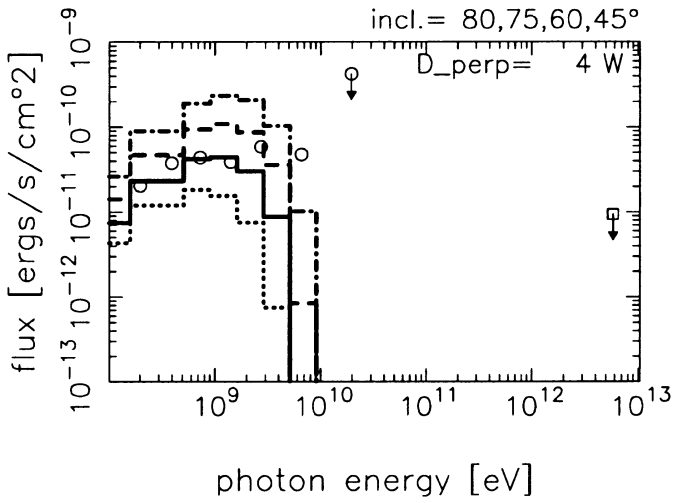


FIG. 10.—Expected pulsed $\gamma$-ray spectra from PSR B1055−52 for 45° (*dotted curve*), $\alpha_i = 60°$ (*solid curve*), 75° (*dashed curve*), and 80° (*dot-dashed curve*). The current densities are fixed as $j_{gap} = 0.01$ and $j_1 = j_2 = 0$. In all the four cases, outwardly propagating fluxes are greater than (or dominate) the inwardly propagating ones.

2. The magnetic field strength, and hence the Goldreich-Julian charge density, $\Omega B_z/(2\pi c)$, in the gap increases as the distance from the star decreases.

3. It follows from the Poisson equation that the derivative of $-d\Psi/ds$ (i.e., $-d^2\Psi/ds^2$) increases with increasing $B_z$ (i.e., with decreasing distance from the star).

4. By virtue of this increasing derivative, the acceleration field $-d\Psi/ds$ at the gap center increases. We may notice here that $W$ does not decrease very rapidly with increasing $\alpha_i$ because of the "negative" feedback effect due to the $N_\gamma$ factor in equation (27). As a result of this increased $-d\Psi/ds$, the spectrum becomes hard for a large $\alpha_i$.

It is worth noting that the Tev flux is always negligibly small compared to the observational upper limit. This is because the infrared flux, which is deduced from the Rayleigh-Jeans side of the soft surface blackbody spectrum, declines sharply as $\nu^2$ at small frequency, $h\nu \ll kT_s$.

### 3.4. *Dependence on Distance*

We have assumed that the distance is 0.5 kpc so that the observed area of the soft blackbody emission, $A_s = 0.78A_*(d/0.5\ \text{kpc})^2$, may be less than $A_*$. In this section, we consider the case in which the distance is 1.5 kpc, as indicated by Taylor, Manchester, & Lyne (1993), and compare the results with the $d = 0.5$ kpc case.

In Figure 11, we present the resultant spectra for $\alpha_i = 80°$, $j_{gap} = 0.01$, and $j_1 = j_2 = 0$. The solid (or dashed) line represents the $\gamma$-ray spectrum when the distance is 0.5 kpc (or 1.5 kpc). The normalization is adjusted by the fluxes below 0.5 GeV; namely, the cross sectional area $D_\perp^2 = 2.3^2W^2$ (or $7.7^2W^2$) is assumed for $d = 0.5$ kpc (or 1.5 kpc). It is clear from Figure 11 that the GeV spectrum becomes hard if we assume a smaller distance $d$.

The conclusion that a small distance to this pulsar is preferable is derived because the less dense X-ray field for a smaller $d$ results in a larger $\lambda_p$ in equation (27) and hence in a larger $W$; a large $W$ results in a strong acceleration field, which leads to a hard spectrum. However, the solution does not vary so much even though the X-ray density increases

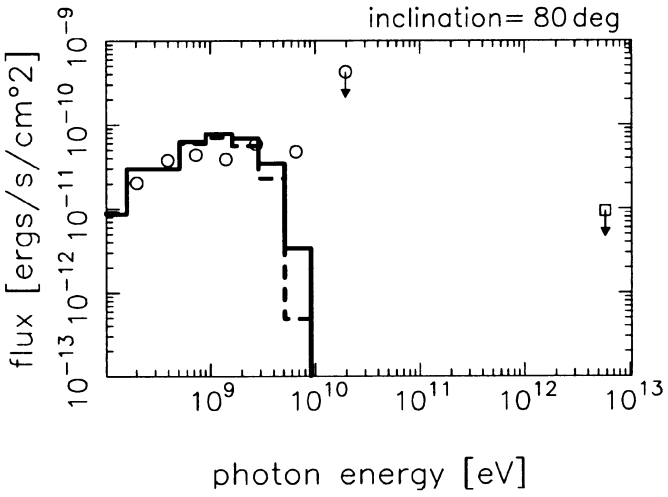


FIG. 11.—Expected pulsed $\gamma$-ray spectra from PSR B1055−52 for $\alpha_i = 80°$, $j_{\rm gap} = 0.01$, and $j_1 = j_2 = 0$. The solid (or dashed) line represents the $\gamma$-ray spectrum when the distance is 0.5 kpc (or 1.5 kpc).

(1.5 kpc/0.5 kpc)$^2 = 9$ times. This is due to the negative feedback effect caused by the $N_\gamma^{-1}$ factor in equation (27); that is, the increase of $W$ is substantially canceled by the increase of $N_\gamma$, which is proportional to the product of the curvature radiation rate of a particle per unit length and $W$. In other words, the solution exists for a wide range of parameters and does not change very much if the variation of the X-ray field density is within 1 order of magnitude.

## 4. DISCUSSION

In summary, we have developed a one-dimensional model for an outer gap accelerator in the magnetosphere of a rotation-powered pulsar. Solving the Vlasov equations that describe a stationary pair production cascade, we revealed that the accelerator shifts toward the star surface (or the light cylinder) as the particle injection rate across the outer (or inner) boundary approaches the Goldreich-Julian value. Applying this theory to a middle-aged pulsar, B1055−52, we find that stationary solutions exist for a wide range of parameters such as the injected currents, magnetic inclination, and distance to the pulsar. Comparing the expected spectrum with EGRET observations, we conclude that a sub–Goldreich-Julian current density, a large magnetic inclination, and a small distance (500 pc, say) are preferable for this pulsar.

### 4.1. *Created Current as a Free Parameter*

In this subsection, let us discuss the physical reason why $j_{\rm gap}$ should be treated as a free parameter rather than a quantity that is solved from the Vlasov equations. We first consider the vacuum limit in which the true charge density $(B/B_{\rm cnt})(n_+ - n_-)$ in the Poisson equation (eq. [8]) is negligible compared to the Goldreich-Julian charge density $B_z/B_{\rm cnt}$. In this limit, it follows from equations (11) and (14) that if $n_\pm$ and $g^i_\pm$ form a solution of the Vlasov equations, then $f_a n_\pm$ and $f_a g_\pm$ do, as long as the arbitrary factor $f_a$ satisfies $f_a(n_+ - n_-) \ll B_z/B$. It is $j_{\rm gap}$ that parameterizes the arbitrary factor $f_a$.

Next, we consider a nonvacuum gap in which the screening effect due to $(B/B_{\rm cnt})(n_+ - n_-)$ becomes important in the Poisson equation. In this case, the solution deviates from the vacuum as a continuous function of $j_{\rm gap}$ (see Figs. 9 and 10 in Paper I, where $j_0$ in that paper corresponds to $j_{\rm gap}$ in the present paper). The same can be said when the inverse Compton scatterings dominate (Figs. 8, 9, and 10 in Paper II; see also eq. [50], which describes how the voltage drop depends on $j_0$, i.e., $j_{\rm gap}$). The nature of $j_{\rm gap}$ as a free parameter is unchanged if particles are injected from the boundaries. For example, equation (27) shows that the pair production physics determines the gap width as a function of $j_{\rm gap}/j_{\rm tot}$ even if $j_1$ and $j_2$ are fixed.

In the present paper, we are primarily interested in the outer magnetospheric accelerator. Therefore, to emphasize that a gap itself has a freedom, we regard $j_{\rm gap}$ as a free parameter in addition to $j_1$ and $j_2$ and calculate $j_{\rm tot}$ from $j_{\rm tot} = j_{\rm gap} + j_1 + j_2$. However, we may alternatively consider that the total current $j_{\rm tot}$ is determined globally (e.g., in the wind region). In this case, we may have to regard $j_{\rm tot}, j_1$, and $j_2$ as free parameters in an outer gap and calculate $j_{\rm gap}$ from $j_{\rm gap} = j_{\rm tot} - j_1 - j_2$. In other words, $j_{\rm gap}$ may be constrained by a global condition if we consider the polar cap, outer magnetospheric, and wind regions as a whole.

### 4.2. *Maximum Current Density*

We next discuss why there is an upper limit for the current flowing in the gap. It follows from the Poisson equation (eq. [8]) that $dE_\parallel/d\xi$ changes its sign where a space charge is overfilled in the sense that $|n_+ - n_-|$ exceeds $|B_z|/B$ or, equivalently, in the sense that $j_{\rm gap} f_{\rm odd}(x)$ exceeds $(j_1 - j_2) f_{\rm even}(x) + B_z/B$ in equation (30) in Paper VII, where $x$ designates the position in the gap (see § 2 of Paper VII for details).

If the "overfilling" occurs at a certain position, $dE_\parallel/d\xi$ changes its sign there and will diverges outside of the gap (Fig. 2 in Hirotani & Okamoto 1998). Under this circumstance, we obtain two accelerators: the original one and an additional one outside of the point where $E_\parallel$ is minimum. (Usually, such an overfilling occurs close to one of the two boundaries, where $|n_+ - n_-|$ is maximized.) Since $E_\parallel$ diverges in the latter accelerator, a large flux of $\gamma$-rays are expected to illuminate the original gap. The resultant, excessive $\gamma$-ray flux leads to an additional pair production in the gap, which screens the original $E_\parallel$. This screening may continue until $E_\parallel$ closes at the boundaries and, hence, until the additional accelerator vanishes. We conjecture that such a solution having diverging $E_\parallel$ (and, hence, belonging to a higher energy state) is dynamically unstable. We thus consider that there is an upper limit for $j_{\rm gap}$ above which stationary solutions cease to exist because of the overfilling of space charges.

### 4.3. *Pulse Phases at Different Frequencies*

We next consider the expected pulse-phase relationship between the incoherent GeV emission from the outer gap and the coherent radio emission from the polar cap (see, e.g., Michel 1991; Zhang & Harding 2000). If the neutron star is nearly orthogonally rotating ($\alpha_i > 75°$), as indicated in § 3.3 (or Fig. 9), and if the outer gap is located near to the null surface, as indicated in the last paragraph in § 3.2, both the polar cap and outer gap emissions are beamed nearly in the same direction (Fig. 12). It is noteworthy that the intersection of the null surface and the last open field line is located only at $0.0278\varpi_{\rm LC}$ (or equivalently, $8.71 \times 10^{-4}$ s in light crossing time) from the star for $\alpha_i = 80°$. It is therefore possible that the formation of an outer gap near the null surface for a large inclination angle explains the obser-

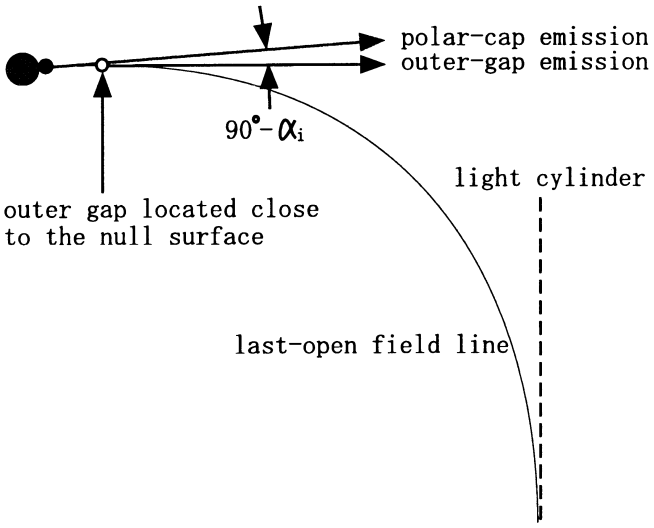


FIG. 12.—Side view of an orthogonal rotator. Radio emissions are supposed to be emitted from the polar cap, while the γ-rays are from the outer gap.

vational fact that the GeV peak in the light curve occurs at the close phase with one of its two radio pulses (Thompson et al. 1999 and references therein).

### 4.4. *Spectrum at Different Positions*

In this subsection, we present the γ-ray spectrum as a function of the position in the gap. As the best-fit case, we choose $\alpha_i = 80°$, $j_1 = j_2 = 0$, and $j_{\rm gap} = 0.01$. To integrate the γ-ray flux in certain regions in the gap, we divide the gap into the following four regions:

*Region 1.*—$1.00\xi_1 + 0.00\xi_2 < \xi < 0.75\xi_1 + 0.25\xi_2$.
*Region 2.*—$0.75\xi_1 + 0.25\xi_2 < \xi < 0.50\xi_1 + 0.50\xi_2$.
*Region 3.*—$0.50\xi_1 + 0.50\xi_2 < \xi < 0.25\xi_1 + 0.75\xi_2$.
*Region 4.*—$0.25\xi_1 + 0.75\xi_2 < \xi < 0.00\xi_1 + 1.00\xi_2$.

In Figure 13, we present the outward γ-ray flux emitted from each region. The dotted, dot-dashed, dashed, and solid lines correspond to the fluxes from regions 1, 2, 3, and 4, respectively. It follows from the figure that the outward

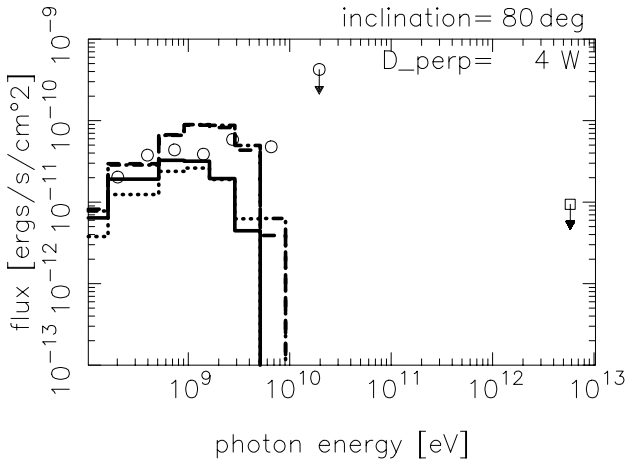


FIG. 13.—Gamma-ray flux from PSR B1055−52 from different positions in the gap, for $\alpha_i = 80°$, $j_{\rm gap} = 0.01$, and $j_1 = j_2 = 0$. The dashed, dot-dashed, dotted, and solid lines represent the $\nu F_\nu$ flux from regions 1, 2, 3, and 4, respectively (see text).

γ-ray fluxes from regions 2, 3, and 4 do not differ very much. However, from region 1, the flux is much smaller than those from other regions. The figure also indicates that the spectrum becomes most luminous hardest from regions 2 and 3 because the electric field is strong there.

### 4.5. *Magnetospheric Current Distribution*

As demonstrated in § 6.3 in Paper VII, the spin-down luminosity of a rotation-powered pulsar becomes (see § 6.3 in Paper VII)

$$\dot{E}_{\rm rot} \sim j_{\rm tot} f_{\rm active}^2 \frac{\Omega^4 \mu_m^2}{c^3}, \tag{29}$$

where $\mu_m$ is the neutron star's magnetic dipole moment and $f_{\rm active}$ represents the ratio of magnetic fluxes along which currents are flowing and those that are open. For PSR B1055−52, $\Omega^4\mu_m^2/c^3 = 10^{34.64}$ ergs s$^{-1}$. If all the open field lines are active (i.e., $f_{\rm active} = 1$), $j_{\rm tot} \sim 1$ is required so that the observed spin-down luminosity $10^{34.48}$ ergs s$^{-1}$ may be realized. If a small fraction of open field lines are active (i.e., $f_{\rm active} \ll 1$), a super–Goldreich-Julian current (i.e., $j_{\rm tot} \gg 1$) is required.

However, our outer gap model requires (and, in fact, previous outer gap models assume) $j_{\rm tot} \ll 1$. Thus, the deficient current must flow along the open field lines that are not threading the accelerator.

### 4.6. *Comparison with Previous Works*

Let us finally compare the present work with the numerical simulation performed by Smith, Michel, & Thacker (2001), who examined equilibrium charge distributions in the magnetosphere of an aligned rotator. In the first place, they demonstrated that the Goldreich-Julian charge distribution is unstable and collapses to form a polar dome containing plasma of one charge and an equatorial belt containing plasma of the other sign: $\boldsymbol{E} \cdot \boldsymbol{B} = 0$ inside both of them. These are separated by a vacuum gap in which $\boldsymbol{E} \cdot \boldsymbol{B} \neq 0$ holds. To apply the theory developed in the present paper to the case in which the Goldreich-Julian charge distribution breaks down, we must modify the Poisson equation (eqs. [7] and [8]) so that the electric field caused by the charges in the dome and the belt may be taken into account.

In the second place, Smith et al. (2001) demonstrated that the creation of electron-positron pairs in the gap between the dome and the belt reduces the value of $\boldsymbol{E} \cdot \boldsymbol{B}$ in the gap so that it turns off at last. This is because the charges are attracted to regions of the same sign, following the closed field lines, and increasingly filling the magnetosphere. Instead, as considered in the present paper, if pairs are created in the open field line region, we may expect global flows of charged particles and hence a stationary pair production cascade in the magnetosphere of a spinning neutron star. If we extend the work by Smith et al (2001) into oblique rotators and apply the present method to the gap, we may construct a stationary magnetospheric model with pair production cascade under the existence of global currents. There is room for further investigation on this issue.

One of the authors (K. H.) wishes to express his gratitude to Y. Saito and A. K. Harding for valuable advice. He also thanks the Astronomical Data Analysis Center of National Astronomical Observatory, Japan for the use of workstations.

REFERENCES

Beskin, V. S., Istomin, Ya. N., & Par'ev, V. I. 1992, Soviet Astron., 36, 642
Cheng, K. S., Ho, C., & Ruderman, M. 1986a, ApJ, 300, 500 (CHRa)
———. 1986b, ApJ, 300, 522 (CHRb)
Cheng, K. S., Ruderman, M., & Zhang, L. 2000, ApJ, 537, 964
Chiang, J., & Romani, R. W. 1992, ApJ, 400, 629
———. 1994, ApJ, 436, 754
Cohen, R. H. & Treves, A. 1972, A&A, 20, 305
Daugherty, J. K., & Harding, A. K. 1982, ApJ, 252, 337
———. 1996, ApJ, 458, 278
Fierro, J. M., Michelson, P. F., Nolan, P. L., & Thompson, D. J. 1998, ApJ, 494, 734
Greiveldinger, C., Camerini, U., Fry, W., Markwardt, C. B., Ögelman, H., Safi-Harb, S., Finley, J. P., & Tsuruta, S. 1996, ApJ, 465, L35
Harding, A. K., & Muslimov, A. G. 1998, ApJ, 508, 328
Harding, A. K., Tademaru, E., & Esposito, L. S. 1978, ApJ, 225, 226
Hirotani, K. 2000a, MNRAS, 317, 225 (Paper IV)
———. 2000b, PASJ, 52, 645 (Paper VI)
———. 2001, ApJ, 549, 495 (Paper V)
Hirotani, K. & Okamoto, I. 1998, ApJ, 497, 563
Hirotani, K. & Shibata, S. 1999a, MNRAS, 308, 54 (Paper I)
———. 1999b, MNRAS, 308, 67 (Paper II)
———. 1999c, PASJ, 51, 683 (Paper III)
———. 2001a, ApJ, 558, 216 (Paper VII)
———. 2001b, MNRAS, 325, 1228 (Paper VIII)
Holloway, N. J. 1973, Nature, 246, 6
Holloway, N. J. 1977, MNRAS, 181, 9
Kanbach, G., et al. 1994, A&A, 289, 855
Kaspi, V. M., Lackey, J. R., Manchester, R. N., Bailes, M., & Pace, R. 2000, ApJ, 528, 445
Mayer-Hasselwander, H. A., Bertsch, D. L., Brazier, T. S., Chiang, J., Fichtel, C. E., Fierro, J. M., Hartman, R. C., & Hunter, S. D. 1994, ApJ, 421, 276
Michel, F. C. 1991, ApJ, 383, 808
Mignani, R., Caraveo, P. A., & Bignami, G. F. 1997, ApJ, 474, L51
Nolan, P. L., et al. 1993, ApJ, 409, 697
Ramanamurthy, et al. 1995, ApJ, 447, L109
Romani, R. W. 1996, ApJ, 470, 469
Romani, R. W., & Yadigaroglu, I. A. 1995, ApJ, 438, 314
Rybicki, G. B. & Lightman, A. P. 1979, in Radiation Processes in Astrophysics (New York: Wiley)
Shibata, S. 1995, MNRAS, 276, 537
Shibata, S., Miyazaki, J., & Takahara, F. 1998, MNRAS, 295, L53
Smith, I. A., Michel, F. C., & Thacker, P. D. 2001, MNRAS, 322, 209
Sturner, S. J., Dermer, C. D., & Michel, F. C. 1995, ApJ, 445, 736
Taylor, J. H., Manchester, R. N., & Lyne, A. G. 1993, ApJS, 88, 529
Thompson, D. J., et al. 1999, ApJ, 516, 297
Thompson, D. J., Bailes, M., Bertsch, D. L., Esposito, J. A., Fichtel, C. E., Harding, A. K., Hartman, R. C., & Hunter, S. D. 1996, ApJ, 465, 385
Zhang, B., & Harding, A. K. 2000, ApJ, 532, 1150
Zhang, L. & Cheng, K. S. 1997, ApJ, 487, 370